THE JOURNAL OF PHYSICAL CHEMISTRY C

Article

Cite This: J. Phys. Chem. C 2019, 123, 8370−8378

pubs.acs.org/JPCC

Competitive Hydrogenation between Linear Alkenes and Aromatics on Close-Packed Late Transition Metal Surfaces

Haoran He,[†] Anish Dasgupta,[†] Robert M. Rioux,[†,‡] Randall J. Meyer,[*,§] and Michael J. Janik[*,†]

[†]Department of Chemical Engineering, The Pennsylvania State University, University Park, Pennsylvania 16801, United States

[‡]Department of Chemistry, The Pennsylvania State University, University Park, Pennsylvania 16801, United States

[§]ExxonMobil Research and Engineering, Annandale, New Jersey 08801, United States

Supporting Information

ABSTRACT: Selective hydrogenation of linear alkenes in the presence of aromatics is desired to prevent gum formation in pyrolysis gasoline (PYGAS) upgrading. To examine the competitive hydrogenation between linear alkenes and aromatics, we investigate ethylene and benzene competitive hydrogenation on different catalysts. Through density functional theory (DFT) calculations, we show the adsorption energies of benzene and ethylene correlate on monometallic close-packed surfaces, with benzene binding stronger for the same C to surface metal atom ratio. DFT calculations demonstrate Brønsted−Evans−Polanyi and scaling relationships hold, and these are fed into microkinetic modeling to predict the rate of ethylene and benzene hydrogenation with only ethylene and hydrogen binding energies as the surface descriptors. Due to stronger binding, benzene adsorption will dominate the surface. Higher barriers for benzene hydrogenation versus ethylene hydrogenation lead to benzene poisoning at temperatures at which ethylene hydrogenation would otherwise have been fast. Experimental studies using a Pd foil catalyst agree with microkinetic model predictions that benzene will poison the surface during ethylene hydrogenation while not being hydrogenated itself. Computational results predict bimetallic surfaces can avoid benzene poisoning during ethylene hydrogenation with the addition of an inert metal to disrupt the binding of benzene on 3-fold sites.

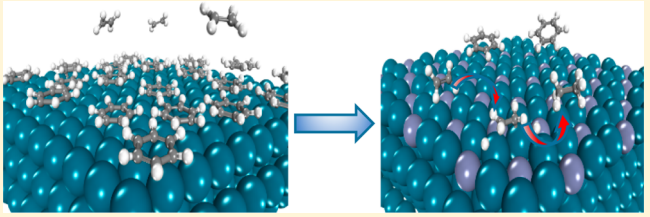

1. INTRODUCTION

Selective hydrogenation, the addition of hydrogen to certain chemical functionalities, while leaving others unperturbed, is an important catalytic process for the production of many hydrocarbon fuels and chemicals. Pyrolysis gasoline (PYGAS), obtained from the thermal decomposition of heavy oil fractions, contains up to 15 wt % gum-forming agents that are mostly linear alkenes, diolefins, and aromatics.[1] In order to prevent gum formation during processing or during storage, the linear alkenes (and dienes) must be hydrogenated.[2] PYGAS composition is complex, containing benzene, toluene, xylene, ethylbenzene, and higher molecular mass aromatics as well as various dienes and alkenes. The design of hydrogenation catalysts that are both active and selective to only the linear alkenes under these conditions remains challenging. Herein, we examine the relative adsorption and hydrogenation of a model alkene (ethylene) and aromatic (benzene) on late transition metal and binary metal surfaces to probe the challenges in attaining the desired selectivity.

The mechanism of ethylene hydrogenation was first proposed by Horiuti and Polanyi in the 1930s, in which ethylene adsorbs on the Pt surface through a di-σ bond at low surface coverage, followed by hydrogenation to ethane in a stepwise manner.[3] A more detailed description of ethylene hydrogenation has been developed from thorough mechanistic examination on single crystal surfaces. Somorjai and coworkers identified π-bonded ethylene as the primary intermediate and ethylidyne as a spectator species during hydrogenation through application of sum frequency generation (SFG) surface vibrational spectroscopy.[4] Pallassana et al. used density functional theory (DFT) to study ethylene hydrogenation on Pd monolayers and found ethylene hydrogenation activation barriers and reaction enthalpies correlated with the surface d-band center energy.[5] Dumesic et al. explored ethylene hydrogenation kinetics on Pt catalysts and found hydrogen and ethylene compete for sites at higher temperature but adsorb noncompetitively at low temperature.[6,7] These studies are consistent with the Horiuti and Polanyi mechanism. In our density functional theory (DFT) analysis, we assume ethylene hydrogenation follows the Horiuti−Polanyi mechanism.

The benzene hydrogenation mechanism is more complicated, as six C−H formation steps lead to a multitude of possible adsorption configurations and reaction paths. The hydrogenation sequence of the six carbon atoms has not been definitively determined and may vary across transition metals.

Special Issue: Hans-Joachim Freund and Joachim Sauer Festschrift

Received: September 30, 2018
Revised: December 3, 2018
Published: December 7, 2018

DOI: 10.1021/acs.jpcc.8b09564
J. Phys. Chem. C 2019, 123, 8370−8378

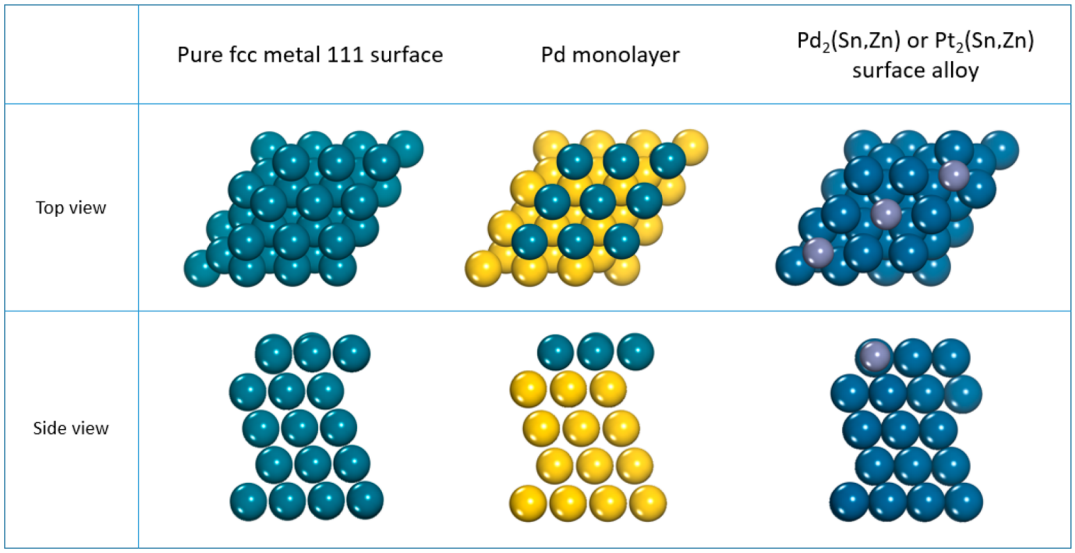

Figure 1. Three classes of catalytic surfaces considered with DFT calculations.

Though a large number of experimental techniques have been applied to examine benzene adsorption on Ru, Rh, Ni, Cu, and Pt catalysts, the exact adsorption site is still debated. Scanning tunneling microscopy (STM) and DFT studies revealed benzene preferentially adsorbs on Pt(111) with the center of the molecule above a bridge site at low coverage and above a 3-fold hollow site at high coverage.[8−10] On Ru(0001), low energy electron diffraction (LEED) analysis indicated the hcp site is preferred for coverages ranging from 0.083 to 0.143 ML (1 ML is one adsorbed molecule per surface Ru atom).[11] On Ni(111), similar to Pt, benzene prefers bridge sites at low coverage and hcp sites at high coverage, as demonstrated by photoelectron diffraction (PED).[12] Apart from the complexity of possible adsorption configurations, the benzene hydrogenation path has not been conclusively identified. Vannice et al. proposed sequential addition of H atoms to the benzene ring and comparable activation barriers among hydrogenation steps on supported and unsupported Pd.[13] Liu et al. concluded stepwise hydrogenation of neighboring C atoms based on a DFT study of benzene hydrogenation activation barriers and reaction energies.[14] Saeys et al. demonstrated meta-position hydrogenation was the dominant reaction path using DFT calculations of the activation energies for all of the possible elementary steps.[15] For the sake of simplicity, we studied benzene hydrogenation based on sequential C−H formation of neighboring C atoms.

To our knowledge, the competitive hydrogenation of benzene and ethylene has not previously been considered. Benzene hydrogenation typically occurs at higher temperature than ethylene. For example, benzene hydrogenation requires a temperature of 370 K with an activation barrier of 12 kcal/mol, whereas ethylene can hydrogenate readily at 227 K with a barrier of 3 kcal/mol on Pd catalysts.[13,16] The higher barriers for benzene hydrogenation are due to the need to break the aromaticity of the ring. We expect the ethylene hydrogenation rate constant will exceed the benzene hydrogenation rate constant at the same temperature. However, benzene also binds to the surface more strongly than ethylene, as it can form six carbon metal bonds and has stronger van der Waals interaction with the surface. Stronger adsorption allows benzene to outcompete ethylene for sites on the surface. These factors will compete to dictate the relative hydrogenation rates when ethylene and benzene are co-fed.

In this work, we apply density functional theory to examine the selective hydrogenation of ethylene versus benzene over several transition metals and bimetallic catalysts. A microkinetic model has been constructed to simulate competitive hydrogenation under relevant industrial conditions. We also report initial experiments of ethylene hydrogenation in the presence of benzene over a Pd catalyst.

2. METHODS

2.1. Electronic Structure Methods. Electronic structure calculations were performed using the Vienna ab initio simulation package (VASP).[17] The projector augmented-wave (PAW) method was used to represent the ion−core electron interactions.[18] The valence electrons were represented with a plane wave basis set with an energy cutoff of 450 eV. Nonlocal gradient corrections to the total energy were calculated using the Perdew−Burke−Ernzerhof (PBE) exchange correlation functional.[19] A 4 × 4 × 1 Monkhorst−Pack scheme was used to generate the *k*-point grid for our 3 × 3 and $\sqrt{3} \times \sqrt{3}$ supercells of fcc (111) surfaces.[20] The structural convergence criteria was 0.05 eV Å^{-1} for all unconstrained atoms. The transition states were obtained using the climbing image nudged elastic band (CI-NEB) method with the transition state identified to have an absolute tangent force below 0.05 eV/Å.[21] Inclusion of dispersion interactions was shown to be necessary to match experimental adsorption energies for similar molecules.[22] We performed all of the surface calculations using the PBE functional with dispersion correction and PBE-D3 with Becke−Jonson damping.[23−25] Zero-point vibrational energy (ZPVE) corrections are included for all reported energetics

$$E = E_{\mathrm{DFT}} + E_{\mathrm{ZPVE}} \quad (1)$$

where E_{DFT} is the energy obtained from an electronic structure calculation and E_{ZPVE} is the zero-point vibrational energy. The ZPVE corrections were calculated for structures on the Pd(111) surface, and the same correction was then applied across all metals, as adsorbate and transition structures are very similar across all the close-packed metal surfaces considered.

DOI: 10.1021/acs.jpcc.8b09564
J. Phys. Chem. C 2019, 123, 8370−8378

We considered three different classes of metal surface slabs, as shown in Figure 1. The first is pure fcc transition metal (111) surfaces, including Ir, Pd, Pt, Ni, Rh, Ag, Au, and Cu. These include typical hydrogenation catalysts as well as relatively inert metals that do not chemisorb benzene and ethylene due to their nearly full d-band structure. The second class of metal surfaces we considered is Pd monolayers over Ag(111), Au(111), Ir(111), Pt(111), Re(111), and Ru(0001) surfaces. Among those substrates, Au, Re, and Ru were studied by Pallassana el al. to investigate the effect of substrate on the Pd monolayer electronic structure and hydrogenation activity.[5] In these overlayer models, we first optimized the five-layer substrate model and then replaced the top layer with Pd and reoptimized the surface slab. There are no significant surface reconstructions observed during optimization. The third class of surfaces considered is Zn or Sn doped Pd(111) and Pt(111) surfaces, denoted as Pd_2Zn_1, Pd_2Sn_1, Pt_2Zn_1, and Pt_2Sn_1. These surface alloys were constructed by replacing one of every three Pd atoms in the top surface layer with Zn or Sn atoms, such that all 3-fold sites have one Zn or Sn atom. These surfaces allow evaluation of the impact of distributed inert metal atoms on the adsorption and hydrogenation of ethylene and benzene. All slab models are composed of five metal layers, in which the bottom three layers were fixed at the optimized bulk lattice constant and the top two layers were allowed to relax. To consider competitive adsorption between benzene and ethylene, we used 3×3 supercells for benzene and $\sqrt{3} \times \sqrt{3}$ supercells for ethylene to examine the adsorption behavior of these species at the same carbon/metal coverage. A vacuum layer of 12 Å was included between surface slabs to ensure there were negligible interactions between adsorbate and the neighboring surface slab.

Adsorption energies of benzene and ethylene were calculated as

$$\Delta E_{ads} = E_{tot} - E_{sur} - E_{mol} \quad (2)$$

where E_{tot} is the total energy of benzene and ethylene on the surface, E_{sur} is the energy of the bare surface, and E_{mol} is the energy of the molecule (ethylene or benzene) in a vacuum. When we calculate adsorption free energy, a typical gas phase entropy of 0.002 eV/K is applied, which is also used by Nørskov et al.[26] We examined the sensitivity to small changes in this value and found no changes that impacted the conclusions reached.

Reaction energies (ΔE_{rxn}) and activation barriers (ΔE_{act}) are defined as

$$\Delta E_{rxn} = E_{final} - E_{initial} \quad (3)$$

where E_{final} represents the final state energy and $E_{initial}$ is the initial state energy and

$$\Delta E_{act} = E_{TS} - E_{initial} \quad (4)$$

where E_{TS} is the energy of the transition state.

2.2. Microkinetic Model. We used microkinetic modeling to predict the relative rates of benzene and ethylene hydrogenation across the range of catalysts. The steady state elementary hydrogenation reaction rates were calculated as

$$r_i = \frac{k_B T}{h} \exp\left(\frac{-\Delta G_i^{act}}{RT}\right) \theta_i \theta_H \quad (5)$$

where k_B is the Boltzmann constant, T is the temperature, h is Planck's constant, ΔG_i^{act} is the activation barrier of elementary step i, and θ_i and θ_H are fractional coverages of species i and H atoms.

Across all catalysts, we did not find any appreciable formation rate of benzene hydrogenation products other than cyclohexane. We did not consider any C−C bond cleavage/formation in our model. Therefore, the only products formed are ethane and cyclohexane.

We calculated desorption rate constants by setting the desorption barrier equal to the DFT desorption energy, with the pre-exponential factor for k_{des} given by $\frac{k_B T}{h}$. We did not include any increase in the available translational entropy at the desorption transition state. Product (ethane, cyclohexane) desorption was rapid, and reactant adsorption was equilibrated such that an increase in the desorption rate constants would not affect the present kinetic results. The adsorption rate constant was calculated as the product of the desorption rate constant and the adsorption equilibrium constant, obtained from the adsorption free energy. Our microkinetic model is quite simplified by neglecting phenomena such as the coverage dependent adsorption energies of ethylene and benzene (which could tilt from the surface plane at high coverages) as well as neglecting the possible formation of spectator species (such as ethylidyne) not directly involved in the mechanisms considered.

2.3. Experimental Details. All reactions were performed in a fritted tubular flow reactor with ∼10 mm I.D. (ChemGlass). A Pd foil (2×2 mm^2, mixed with 60 mg of silica gel (Sigma-Aldrich, Davisil grade 62, 60−200 mesh)) was used as a model catalyst to examine the competitive hydrogenation of ethylene and benzene. For all experiments, the catalyst temperature was maintained at 180 °C. This is consistent with our microkinetic model and is also sufficiently high to overcome the activation barrier toward the hydrogenation of both ethylene and benzene but low enough that cyclohexene or cyclohexane dehydrogenation is unfavorable.[27−30] Benzene (EM Science) was introduced into the reactor by bubbling He via a mass flow controller (Tylan) through a saturator (ChemGlass) containing benzene maintained at 7 °C by an external chiller (Fisher Scientific). The benzene partial pressure was controlled by changing the flow rate of the carrier He (Praxair, ultrahigh purity (UHP)). All benzene-containing lines were wrapped in heat tape and held at ∼85 °C to prevent any condensation of benzene within the lines. The reactant gas consisted of 16 Torr of ethylene (Airgas, 10% ethylene in He) and 130 Torr of hydrogen (Praxair, UHP), with the balance a combination of benzene (delivered by the carrier He (UHP)) and (another separately controlled) He (Praxair (UHP)) stream such that the total flow rate was 60 mL/min. The Pd foil was reduced *in situ* at 250 °C in hydrogen for 2 h and then held at the same temperature for 20 min in He (in order to eliminate any Pd hydride) before cooling under He to the reaction temperature. The Pd foil was equilibrated at the reaction temperature for 30 min in He before switching the flow to the reactant mixture. Effluent gas was analyzed by online gas chromatography (Agilent 7890). A GS-Alumina PLOT column (Agilent Technologies, l = 30 m, d = 0.53 mm) was used.

3. RESULTS AND DISCUSSION

We first report DFT results for the adsorption of ethylene and benzene. We calculate hydrogenation barriers and show a Brønsted−Evans−Polanyi (BEP) relationship for ethylene and

DOI: 10.1021/acs.jpcc.8b09564
J. Phys. Chem. C 2019, 123, 8370−8378

benzene hydrogenation, which simplifies the microkinetic model construction. Combining both calculated adsorption energies and hydrogenation reaction barriers, a microkinetic model for competitive hydrogenation between ethylene and benzene under various conditions is reported, followed by experimental competitive hydrogenation results.

3.1. Ethylene and Benzene Competitive Adsorption. We studied benzene and ethylene adsorption on atop, bridge, and hollow sites. Our calculation showed benzene prefers to bind on bridge sites on most metals forming two π bonds and two σ bonds and to physisorb on coinage metals (Au(111), Ag(111), Cu(111)), as reported by other researchers.[22,31−33] Ethylene prefers to adsorb to a bridge site on Ir, Pd, Pt, Pd/Ag, Pd/Au, Pd/Ir, and Pd/Pt, forming a di-σ bond, and an atop site on Rh, forming a π bond, in good agreement with the literature.[5,34,35] For benzene adsorption energies on Ag, Pd, Rh, Ir, Au, and Pt, our calculation results are in excellent agreement with Liu's study.[22] Figure 2 shows ethylene and benzene binding energies on the energetically most favorable sites, for which there exists a linear correlation between the benzene and ethylene binding energies. The linear correlation is not surprising, as both benzene and ethylene are unsaturated planar hydrocarbon molecules that adsorb through their π bonds. Linear correlations exist between ethylene and benzene binding energies on atop, bridge, and hollow sites, respectively (see the Supporting Information). These linear correlations can be attributed directly to an electronic effect, since the adsorption energy can be correlated to the d-band center of the metal.[5,36]

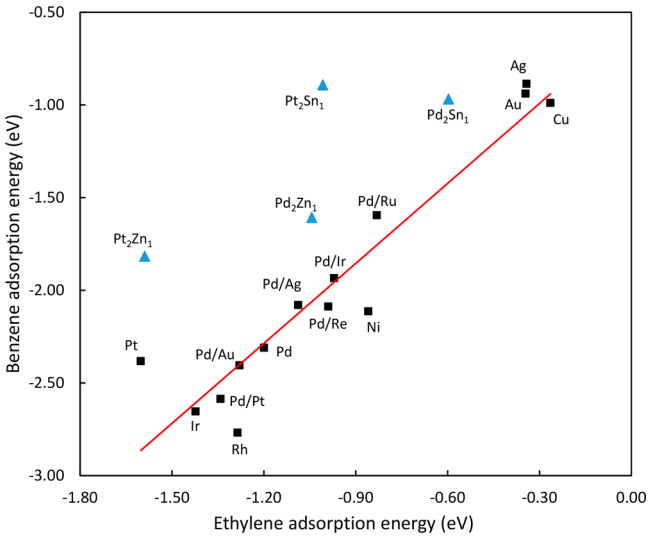

Figure 2. Linear correlation between ethylene adsorption energies on $\sqrt{3} \times \sqrt{3}$ metal surfaces and benzene adsorption energies on 3 × 3 metal surfaces. The linear best fit to the pure metal surface data is $E_{ads}^{benzene} = 1.44E_{ads}^{ethylene} - 0.56$ eV, with an R^2 value of 0.90 and a mean absolute error (MAE) of 0.14 eV. The blue triangles represent ethylene and benzene adsorption on surface alloys, which have not been included in the linear correlation.

As shown in Figure 2, benzene binds more strongly than ethylene to all single metal surfaces, at the same carbon to surface metal molar ratio of 2:3. The slope of approximately 1.5 shows that stronger binding leads to a larger preference for benzene, with the value of the slope consistent with the interaction of benzene with three surface metal atoms versus two for ethylene. Therefore, we expect benzene to outcompete ethylene for surface sites (i.e., poison the surface) when co-fed during competitive hydrogenation.

Ideally, tuning the selectivity for ethylene or benzene hydrogenation could be done by designing active sites that could adsorb only a single type of adsorbate on the surface. The linear correlation in Figure 2 suggests independent tuning of binding will be challenging, since benzene always adsorbs more strongly regardless of metal or binding site. Therefore, we explored whether surface alloys involving inactive Sn and Zn could break this linear correlation by breaking up the larger adsorption site ensemble required to bind benzene. Figure 2 includes the adsorption energy of benzene and ethylene on four surface alloys. Addition of Zn or Sn breaks the ensemble for benzene adsorption such that these four points deviate from the linear correlation. On these surface alloys, no 3-fold hollow sites composed only of the late transition metal exist. In contrast to benzene, the adsorption of ethylene was not affected as substantially, since it requires a smaller ensemble of adsorption sites, typically one to two metal atoms. On Pt_2Sn_1, ethylene adsorption is stronger than benzene adsorption. We have effectively changed the relative binding strengths of ethylene and benzene by tuning the size of the active site ensemble, which could affect selectivity during competitive hydrogenation by altering the relative surface coverages. Doping the inactive component into the surface should favor ethylene hydrogenation, since it weakens the adsorption of benzene significantly. Such surface alloys may be useful in selectively hydrogenating linear alkenes in the presence of aromatics, reducing both aromatic hydrogenation and self-poisoning by the aromatic.

3.2. Ethylene Hydrogenation Elementary Step Energetics. DFT was used to determine activation barriers for the elementary steps in the hydrogenation of ethylene for use in the subsequent ethylene/benzene competitive hydrogenation microkinetic model. Hydrogenation transition states were considered using the most stable ethylene adsorption configuration; the di-σ adsorption mode was used for the adsorbed ethylene initial state on the Pd monolayer (Pd(111)/Ag(111), Pd(111)/Au(111), Pd(111)/Ir(111), Pd(111)/Pt(111), Pd(111)/Re(111), and Pd(111)/Ru(0001)) and the pure transition metals (Pd(111), Pt(111), Ir(111), and Ni(111)). The π adsorption mode was used on Rh(111). Our calculated activation barriers on Pt are slightly higher than those reported by Heard et al., because they started with ethylene adsorbed in the less stable π-bonded mode.[37] As shown in Figure 3, a linear correlation between the activation barrier and the reaction energy exists for ethylene hydrogenation. Neurock and co-workers have reported a BEP relationship in their study of ethylene hydrogenation over Pd monolayers.[5] From the linear correlation, we can derive activation barriers from reaction energies, which reduces the number of variables in our microkinetic model. The slope of ~0.5 indicates the transition states lie in the middle of initial and final states. The ethylene hydrogenation on Pt_2Sn_1 does not fall on the BEP line, with a higher activation barrier due to disruption of the larger ensemble site needed for C−H bond formation. This demonstrates a trade-off; reduced adsorption energies of aromatics on alloys are accompanied by a reduced activity for alkene hydrogenation. However, the ethylene hydrogenation on Pd_2Zn_1 still falls onto the BEP line, as the active site ensemble disruption of Zn is not as significant as Sn, which can also be reflected by adsorption in Figure 2.

DOI: 10.1021/acs.jpcc.8b09564
J. Phys. Chem. C 2019, 123, 8370−8378

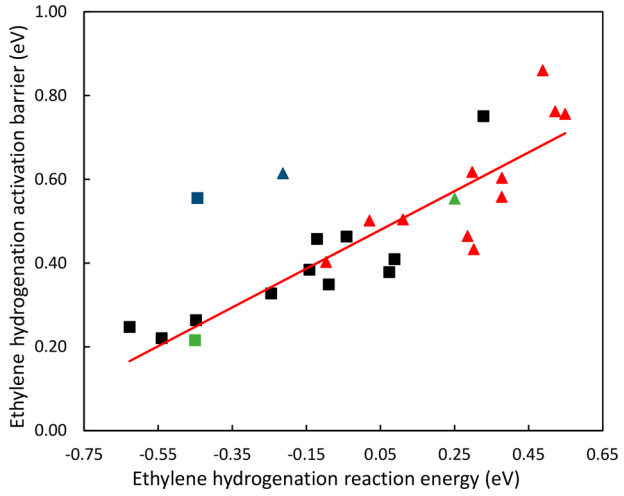

Figure 3. Ethylene hydrogenation BEP relation, $\Delta E^{act} = 0.46\Delta E^{rxn} + 0.46$ eV, with an R^2 value of 0.78 and MAE of 0.06 eV. Triangles represent ethylene hydrogenation barriers for ethyl formation (first step), and squares represent the hydrogenation barrier for ethane formation (second step). The blue triangle and square represent the first and second hydrogenation of ethylene on Pt_2Sn_1. The green triangle and square represent the first and second hydrogenation of ethylene on Pd_2Zn_1. Exact numbers are shown in Table S1.

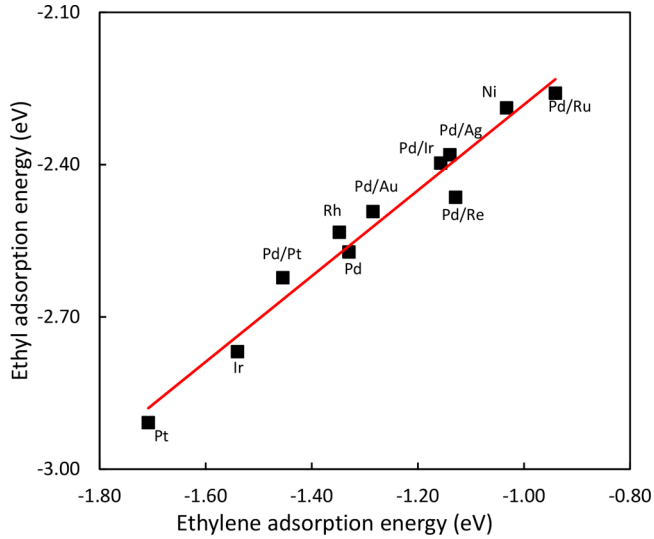

Figure 5. Linear correlation between the adsorption energy of ethylene and ethyl. The linear fit to the pure metal surface data is $E_{ads}^{ethyl} = 0.84E_{ads}^{ethylene} - 1.44$ eV, with an R^2 value of 0.96 and MAE of 0.03 eV.

Activation barriers can be obtained from the BEP relation, but calculation of reaction enthalpies still requires optimizing the initial and final states. To further simplify our microkinetic model, we demonstrate reaction enthalpies can be predicted on the basis of ethylene and H adsorption energies. The thermochemical cycle in Figure 4 illustrates our approach to predict reaction enthalpies by taking advantage of scaling relationships between the adsorption energies of ethylene, ethyl, and ethane species. The first (ΔE_{rxn1}) and second (ΔE_{rxn2}) ethylene hydrogenation elementary step reaction energies can be written as

$$\Delta E_{rxn1} = -\Delta E_{adsC_2H_4} - \Delta E_{adsH} + \Delta E_{rxn1(g)} + \Delta E_{adsC_2H_5} \quad (6)$$

$$\Delta E_{rxn2} = -\Delta E_{adsC_2H_5} - \Delta E_{adsH} + \Delta E_{rxn2(g)} + \Delta E_{adsC_2H_6} \quad (7)$$

Montemore et al. established a scaling relation for hydrocarbons on hexagonal (fcc and hcp) transition metals.[38] Similarly, we found the adsorption energy of ethyl is linearly correlated with the ethylene adsorption energy (Figure 5). Ethane adsorption is weak and nearly constant over the various metals considered, as the adsorption energy is due almost solely to the van der Waals interaction with the saturated alkane. Equation 6 shows that linear scaling of the ethyl and ethylene adsorption energies allows us to calculate (ΔE_{rxn1}) directly from the ethylene and hydrogen adsorption energies. Equation 7 similarly shows that ethyl and ethane adsorption scaling with the ethylene adsorption energy reduces the catalyst descriptors to ethylene and hydrogen adsorption energies. Note that all gas phase species energies cancel in eqs 6 and 7, so their energies do not appear in the surface reaction energies. Combining scaling relationships with the BEP relationship enables the prediction of all ethylene hydrogenation reaction energies and activation barriers, given the adsorption energies of ethylene and H on the pure metal surfaces.

3.3. Benzene Hydrogenation Elementary Step Energetics. DFT calculations were used to determine the elementary reaction energetics and activation barriers for benzene hydrogenation to cyclohexane. We use benzene adsorbing on a hollow site, which is the energetically most favorable on most of the (111) surfaces and allows stable surface packing at high coverage.[39] We assumed hydrogenation occurs sequentially on neighboring carbon atoms in our DFT calculations. Figure 6 is a BEP relationship for benzene hydrogenation on Pd(111), Pt(111), and Ir(111) surfaces, including all six hydrogenation steps on each surface. The slope of 0.57 demonstrates the transition states for each of the six hydrogenation steps possess a transition state intermediate between reactant and product states. The first hydrogenation step has a high barrier, but it does not function as the rate

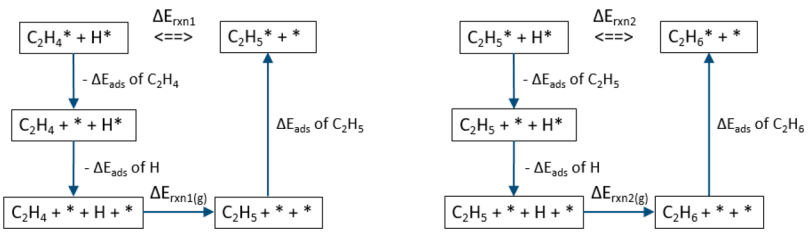

Figure 4. Thermochemical cycle for the elementary steps of ethylene hydrogenation illustrating the relationship between elementary reaction energies and the binding energies of reactants and products. Asterisks designate surface sites or adsorbed species.

DOI: 10.1021/acs.jpcc.8b09564
J. Phys. Chem. C 2019, 123, 8370−8378

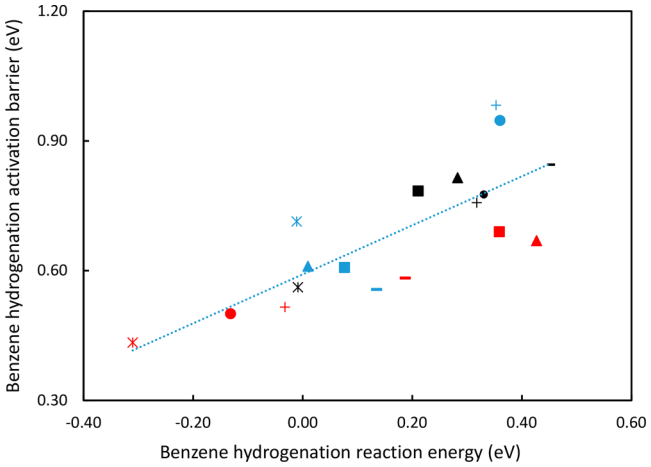

Figure 6. BEP relationship for the sequential hydrogenation of benzene. $\Delta E^{act} = 0.57\Delta E^{rxn} + 0.59$ eV. Six hydrogenation steps on Pd (red), Ir (black), and Pt (blue) data presented, with an R^2 value of 0.62 and MAE of 0.07 eV. The first steps ($C_6H_6^* + H^* \rightarrow C_6H_7^* + *$) are represented by squares; the second steps ($C_6H_7^* + H^* \rightarrow C_6H_8^* + *$) are represented by triangles; the third steps ($C_6H_8^* + H^* \rightarrow C_6H_9^* + *$) are represented by circles; the fourth steps ($C_6H_9^* + H^* \rightarrow C_6H_{10}^* + *$) are represented by horizontal lines; the fifth steps ($C_6H_{10}^* + H^* \rightarrow C_6H_{11}^* + *$) are represented by crosses; the sixth steps ($C_6H_{11}^* + H^* \rightarrow C_6H_{12}^* + *$) are represented by stars.

limiting step. The net hydrogenation enthalpy relative to the surface bound benzene state is positive, and therefore, subsequent barriers appear higher on the potential energy surface and dictate the apparent barrier, as shown in the Supporting Information (Figure S2). We include all six benzene hydrogenation steps in our microkinetic model.

Similar to the linear correlation observed between ethyl and ethylene adsorption energies, benzene hydrogenation intermediate adsorption energies linearly correlate with each other, and, therefore, correlate linearly with ethylene due to the benzene−ethylene correlation in Figure 2. These correlations are shown in Figure S3. Combined with the BEP relationship in Figure 6, we can correlate all of the barriers for benzene hydrogenation directly to the adsorption energy of ethylene and hydrogen.

3.4. Benzene and Ethylene Competitive Hydrogenation Microkinetic Model. A microkinetic model was constructed including ethylene, benzene, and dissociative H_2 adsorption and all elementary steps for hydrogenation of ethylene to ethane and benzene to cyclohexane. Only the ethylene and H adsorption energies are needed to determine all of the barriers for both hydrogenation reactions, using the scaling and BEP relationships discussed in previous sections. We used a dual-site model, in which H adsorbs on one type of site and benzene and ethylene adsorb competitively on the other site. The dual-site model is based on consideration of the molecular size difference between H atoms and ethylene or benzene molecules. A similar "dual-site" mechanism was applied in previous hydrogenation studies, showing good agreement with experimental results.[7,28] On the basis of the preferred adsorption configuration, we assume benzene occupies 1.5 sites while ethylene occupies a single site, effectively defining a site as composed of two surface metal atoms. We assume the number of sites available for H equals that available to ethylene and benzene.

Figure 7 shows ethane and cyclohexane formation rates in the presence of benzene, ethylene and hydrogen. The reaction conditions are 500 K, partial pressure of hydrogen of 12 atm, partial pressure of ethylene of 2 atm, and partial pressure of benzene of 2 atm. Both the ethylene and benzene hydrogenation rates have a volcano shape, which indicates intermediate binding energies of the reactants will yield the highest reaction rate. This is because too weak binding leads to low surface coverage, whereas too strong binding leads to larger activation barriers. Though benzene coverage greatly exceeds that of ethylene for all catalysts (Figure S4), the higher barrier for hydrogenation leads to very low rates of cyclohexane formation. Therefore, the main effect of co-feeding benzene and ethylene is poisoning of the surface by benzene to reduce the rate of ethylene hydrogenation. The ethylene hydrogenation rate exceeds benzene hydrogenation by orders of magnitude, leading to ethane selectivity >99% for all catalysts.

We also examined a microkinetic model for ethylene hydrogenation without co-fed benzene (Figure S5) and observed benzene slows the ethylene hydrogenation rate over all catalysts examined. The optimal binding energy of ethylene shifts to lower values in the presence of benzene. As the benzene adsorption energy correlates with that of ethylene, weaker binding is needed to optimize ethylene hydrogenation to reduce the effect of benzene poisoning when they are co-fed. However, the optimal ethylene hydrogenation catalyst under the co-fed condition is shifted into a region of the plot where no pure metals considered reside.

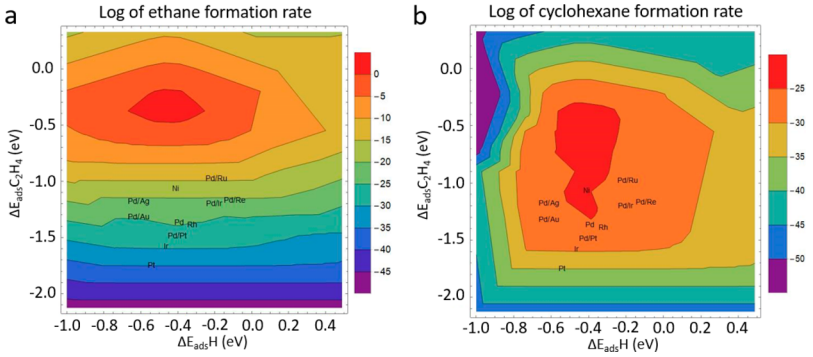

Figure 7. Microkinetic model results for ethane (a) and cyclohexane (b) formation rates from competitive benzene and ethylene hydrogenation. Rates are calculated at 500 K, PH_2 = 12 atm, PC_2H_4 = 2 atm, PC_6H_6 = 2 atm. The rate is expressed as the log base 10 of the rate in units of site^{-1} s^{-1}.

DOI: 10.1021/acs.jpcc.8b09564
J. Phys. Chem. C 2019, 123, 8370−8378

Table 1. Comparison of Ethylene Hydrogenation Rates on Pure Metal Surfaces and Surface Alloys[a]

catalysts	C_6H_6 ΔE_{ads} (eV)	C_2H_4 ΔE_{ads} (eV)	H ΔE_{ads} (eV)	log of ethylene hydrogenation rate without benzene ($\log_{10}^{(\mathrm{TOF}(s^{-1})\ (\mathrm{site}^{-1}))}$)	log of ethylene hydrogenation rate with benzene ($\log_{10}^{(\mathrm{TOF}(s^{-1})\ (\mathrm{site}^{-1}))}$)
Pt(111)	−2.39	−1.72	−0.54	6.2	−34.1
Pt_2Sn_1 using correlation	−2.07	−1.05	−0.13	6.0	−17.6
Pt_2Sn_1 actual	−0.90	−1.05	−0.13	6.3	5.6
Pd(111)	−2.32	−1.21	−0.39	6.7	−23.2
Pd_2Zn_1 using correlation	−2.06	−1.05	−0.30	6.5	--17.7
Pd_2Zn_1 actual	−1.62	−1.05	−0.30	7.2	2.8

[a]Data is included on the basis of the actual binding energies on the surface alloys as well as hypothetical surface alloys for which the correlation of ethylene and benzene binding holds as for pure metal surfaces.

Ethylene and benzene selective hydrogenation on surface alloys (Pd_2Zn_1, Pd_2Sn_1, Pt_2Zn_1, and Pt_2Sn_1) are not plotted in Figure 7, because benzene and ethylene adsorption energies are not correlated such that ethylene and H adsorption energies alone are insufficient descriptors to consider the rates of competitive hydrogenation. Weaker binding of benzene on these surfaces relative to that of the pure metal ethylene−benzene binding correlation could lead to less benzene poisoning. We applied our microkinetic model to examine ethylene hydrogenation on Pt_2Sn and Pd_2Zn surfaces, with and without benzene co-fed. Table 1 shows ethylene hydrogenation rates on the pure metal Pt(111) and Pd(111) surfaces and these two surface alloys. The addition of the inert Zn or Sn into the surface has two major effects. The first is that it weakens the binding energy of both ethylene and benzene, moving Pd or Pt from its pure metal location on the volcano diagram to a weaker binding region. The second effect is that it disrupts the adsorption site of benzene, breaking the correlation of benzene and ethylene binding that was used in making Figure 7. To separate these effects, Table 1 include two lines of data for each of the surface alloys. The first, labeled "using correlation", isolates only the first effect by using the binding energy calculated for ethylene on the surface alloy but approximating that the benzene binding energy correlates with that of ethylene using the correlation found for the pure metal surface. The second, labeled "actual", recognizes that the alloy breaks the correlation of ethylene and benzene binding energy and uses the calculated DFT binding energies and reaction energies and activation barriers of ethylene and benzene on the surface alloy, which are independent from any linear correlation. As these values do not follow the linear correlations used in generating Figure 7, they are not taken from that data but from the equivalent microkinetic model using the actual energetics for the surface alloy.

In the absence of benzene, the pure metal surfaces and alloys show relatively similar ethylene hydrogenation rates, as all appear near the volcano peak. In the presence of benzene, the pure metal surfaces show an extreme reduction in the rate of ethylene hydrogenation due to benzene poisoning. Though these changes in rate likely exceed what would be actually observed, due to our neglect of the coverage dependence of adsorption energies and barriers, this predicted reduction suggests Pt and Pd are poor ethylene hydrogenation catalysts in the presence of benzene at temperatures for which the surface coverage of benzene is appreciable. Addition of Sn or Zn improves the hydrogenation rate in the presence of benzene, even if the correlation of ethylene and benzene adsorption energies is maintained ("using correlation" data in Table 1). This is because the alloy weakens the binding of both species, moving the alloy closer to the peak of the volcano in Figure 7a. However, when the weakened benzene adsorption energies are considered, the rates of ethylene hydrogenation increase even further, nearing those without benzene co-fed on both Pt_2Sn and Pd_2Zn. These microkinetic results suggest that these surface alloys will be considerably less sensitive to benzene poisoning. Such alloys are predicted to selectively hydrogenate ethylene in the presence of benzene without suffering from benzene poisoning, by disrupting the optimal 3-fold site that binds benzene strongly.

3.5. Benzene and Ethylene Competitive Hydrogenation Experimental Results. In an effort to verify the predicted results from the microkinetic model, we co-fed ethylene and benzene in the presence of H_2 over Pd foil and observed the steady-state ethylene conversion as a function of benzene/ethylene ratio (Figure 8). Across the range of benzene/ethylene ratios considered, only ethylene is hydrogenated while benzene is unreactive, leading to a 100% ethane selectivity, consistent with microkinetic model results. The apparent lack of benzene hydrogenation activity of the Pd foil is consistent with the extremely low turnover frequency (TOF) determined by Chou and Vannice on unsupported Pd.[13] It is apparent benzene acts as a surface poison for the hydrogenation of ethylene on Pd. Figure 8 demonstrates ethylene

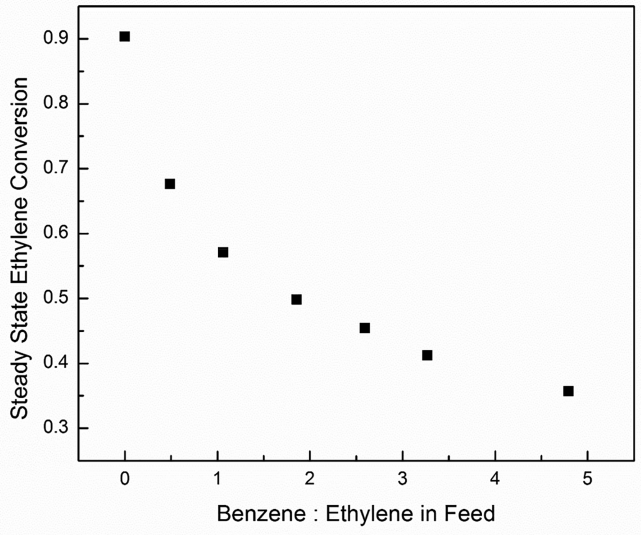

Figure 8. Ethylene conversion as a function of benzene:ethylene ratio in the feed at 180 °C, an ethylene:hydrogen ratio of ~1:8, and an ethylene partial pressure fixed at 16 Torr.

DOI: 10.1021/acs.jpcc.8b09564
J. Phys. Chem. C 2019, 123, 8370−8378

conversion decreases sharply with the introduction of benzene before asymptotically saturating to a nonzero value as the benzene partial pressure is increased. A likely explanation for this observation is that small "pockets" of the Pd surface are available to accommodate both the much smaller ethylene and hydrogen molecules even after benzene has achieved saturation coverage and/or that coverage effects on adsorption energies might predict lower benzene coverages at saturation. These results are qualitatively consistent with the predictions of microkinetic modeling, and in future work, we will experimentally test the computational prediction that alloying Pd with Sn or Zn alleviates/minimizes benzene poisoning during the hydrogenation of ethylene.

4. CONCLUSIONS

We have studied ethylene and benzene adsorption and competitive hydrogenation over a range of transition metals using DFT calculations and microkinetic modeling. Benzene adsorption energies are linearly correlated with ethylene adsorption energies on transition metal (111) surfaces. Idealized surface alloys, such as Pd_2Zn_1, Pd_2Sn_1, Pt_2Zn_1, and Pt_2Sn_1, significantly weakened benzene adsorption, breaking this correlation. Ethylene and benzene hydrogenation BEP relations were found across different transition metals. Microkinetic modeling predicted benzene acts as a poison for the hydrogenation of ethylene, significantly lowering the ethylene hydrogenation rate on most relevant hydrogenation catalysts. Although benzene saturates a majority of the surface sites, its higher hydrogenation barriers lead to little cyclohexane formation at the temperatures considered. This suggests development of catalysts selective for alkene hydrogenation in the presence of aromatics is possible through the addition of inert Sn or Zn into the surface, which could disrupt aromatic poisoning but with a reduction in reaction rate due to a higher barrier for alkene hydrogenation.

■ ASSOCIATED CONTENT

Supporting Information

The Supporting Information is available free of charge on the ACS Publications website at DOI: 10.1021/acs.jpcc.8b09564.

Ethylene hydrogenation reaction enthalpy and activation barrier on each catalyst; linear correlation between ethylene and benzene adsorption energy on different sites; benzene hydrogenation energy diagram; linear correlation between benzene hydrogenation intermediate adsorption energy and ethylene adsorption energy; benzene surface coverage; and ethylene hydrogenation rate without benzene (PDF)

■ AUTHOR INFORMATION

Corresponding Authors

*E-mail: randall.j.meyer@exxonmobil.com.
*E-mail: mjanik@psu.edu.

ORCID

Robert M. Rioux: 0000-0002-6019-0032
Randall J. Meyer: 0000-0002-0679-0029
Michael J. Janik: 0000-0001-9975-0650

Notes

The authors declare no competing financial interest.

■ ACKNOWLEDGMENTS

We acknowledge the US National Science Foundation (NSF Grant No. CBET-1748365) for financial support of this work. H.H. acknowledges training provided by the Computational Materials Education and Training (CoMET) NSF Research Traineeship (Grant No. DGE-1449785). This work used the Extreme Science and Engineering Discovery Environment (XSEDE), which is supported by the National Science Foundation under Grant No. ACI-1548562.

■ REFERENCES

(1) Nijhuis, T. A.; Dautzenberg, F. M.; Moulijn, J. A. Modeling of Monolithic and Trickle-Bed Reactors for the Hydrogenation of Styrene. *Chem. Eng. Sci.* **2003**, *58*, 1113−1124.

(2) Hoffer, B. W.; Bonné, R. L. C.; van Langeveld, A. D.; Griffiths, C.; Lok, C. M.; Moulijn, J. A. Enhancing the Start-up of Pyrolysis Gasoline Hydrogenation Reactors by Applying Tailored Ex Situ Presulfided Ni/Al2o3 Catalysts. *Fuel* **2004**, *83*, 1−8.

(3) Horiuti, I.; Polanyi, M. Exchange Reactions of Hydrogen on Metallic Catalysts. *Trans. Faraday Soc.* **1934**, *30*, 1164−1172.

(4) Cremer, P. S.; Su, X. C.; Shen, Y. R.; Somorjai, G. A. Ethylene Hydrogenation on Pt(111) Monitored in Situ at High Pressures Using Sum Frequency Generation. *J. Am. Chem. Soc.* **1996**, *118*, 2942−2949.

(5) Pallassana, V.; Neurock, M. Electronic Factors Governing Ethylene Hydrogenation and Dehydrogenation Activity of Pseudomorphic Pd-Ml/Re(0001), Pd-Ml/Ru(0001), Pd(111), and Pd-Ml/Au(111) Surfaces. *J. Catal.* **2000**, *191*, 301−317.

(6) Cortright, R. D.; Goddard, S. A.; Rekoske, J. E.; Dumesic, J. A. Kinetic-Study of Ethylene Hydrogenation. *J. Catal.* **1991**, *127*, 342−353.

(7) Rekoske, J. E.; Cortright, R. D.; Goddard, S. A.; Sharma, S. B.; Dumesic, J. A. Microkinetic Analysis of Diverse Experimental-Data for Ethylene Hydrogenation on Platinum. *J. Phys. Chem.* **1992**, *96*, 1880−1888.

(8) Weiss, P. S.; Eigler, D. M. Site Dependence of the Apparent Shape of a Molecule in Scanning Tunneling Microscope Images - Benzene on Pt(111). *Phys. Rev. Lett.* **1993**, *71*, 3139−3142.

(9) Morin, C.; Simon, D.; Sautet, P. Chemisorption of Benzene on Pt(111), Pd(111), and Rh(111) Metal Surfaces: A Structural and Vibrational Comparison from First Principles. *J. Phys. Chem. B* **2004**, *108*, 5653−5665.

(10) Bratlie, K. M.; Kliewer, C. J.; Somorjai, G. A. Structure Effects of Benzene Hydrogenation Studied with Sum Frequency Generation Vibrational Spectroscopy and Kinetics on Pt(111) and Pt(100) Single-Crystal Surfaces. *J. Phys. Chem. B* **2006**, *110*, 17925−17930.

(11) Braun, W.; Held, G.; Steinruck, H. P.; Stellwag, C.; Menzel, D. Coverage-Dependent Changes in the Adsorption Geometries of Ordered Benzene Layers on Ru(0001). *Surf. Sci.* **2001**, *475*, 18−36.

(12) Yau, S. L.; Kim, Y. G.; Itaya, K. In Situ Scanning Tunneling Microscopy of Benzene Adsorbed on Rh(111) and Pt(111) in Hf Solution. *J. Am. Chem. Soc.* **1996**, *118*, 7795−7803.

(13) Chou, P.; Vannice, M. A. Benzene Hydrogenation over Supported and Unsupported Palladium 0.1. Kinetic-Behavior. *J. Catal.* **1987**, *107*, 129−139.

(14) Fan, C.; Zhu, Y. A.; Zhou, X. G.; Liu, Z. P. Catalytic Hydrogenation of Benzene to Cyclohexene on Ru(0001) from Density Functional Theory Investigations. *Catal. Today* **2011**, *160*, 234−241.

(15) Saeys, M.; Reyniers, M. F.; Neurock, M.; Marin, G. B. Ab Initio Reaction Path Analysis of Benzene Hydrogenation to Cyclohexane on Pt(111). *J. Phys. Chem. B* **2005**, *109*, 2064−2073.

(16) Stacchiola, D.; Azad, S.; Burkholder, L.; Tysoe, W. T. An Investigation of the Reaction Pathway for Ethylene Hydrogenation on Pd(111). *J. Phys. Chem. B* **2001**, *105*, 11233−11239.

DOI: 10.1021/acs.jpcc.8b09564
J. Phys. Chem. C 2019, 123, 8370−8378

(17) Kresse, G.; Furthmuller, J. Efficiency of Ab-Initio Total Energy Calculations for Metals and Semiconductors Using a Plane-Wave Basis Set. *Comput. Mater. Sci.* **1996**, *6*, 15−50.
(18) Kresse, G.; Joubert, D. From Ultrasoft Pseudopotentials to the Projector Augmented-Wave Method. *Phys. Rev. B: Condens. Matter Mater. Phys.* **1999**, *59*, 1758−1775.
(19) Perdew, J. P.; Burke, K.; Ernzerhof, M. Generalized Gradient Approximation Made Simple. *Phys. Rev. Lett.* **1996**, *77*, 3865−3868.
(20) Monkhorst, H. J.; Pack, J. D. Special Points for Brillouin-Zone Integrations. *Phys. Rev. B* **1976**, *13*, 5188−5192.
(21) Henkelman, G.; Uberuaga, B. P.; Jonsson, H. A Climbing Image Nudged Elastic Band Method for Finding Saddle Points and Minimum Energy Paths. *J. Chem. Phys.* **2000**, *113*, 9901−9904.
(22) Liu, W.; Carrasco, J.; Santra, B.; Michaelides, A.; Scheffler, M.; Tkatchenko, A. Benzene Adsorbed on Metals: Concerted Effect of Covalency and Van Der Waals Bonding. *Phys. Rev. B: Condens. Matter Mater. Phys.* **2012**, *86*, 245405.
(23) Grimme, S.; Antony, J.; Ehrlich, S.; Krieg, H. A Consistent and Accurate Ab Initio Parametrization of Density Functional Dispersion Correction (Dft-D) for the 94 Elements H-Pu. *J. Chem. Phys.* **2010**, *132*, 154104.
(24) Perdew, J. P.; Burke, K.; Ernzerhof, M. Generalized Gradient Approximation Made Simple (Vol 77, Pg 3865, 1996). *Phys. Rev. Lett.* **1997**, *78*, 1396−1396.
(25) Grimme, S.; Ehrlich, S.; Goerigk, L. Effect of the Damping Function in Dispersion Corrected Density Functional Theory. *J. Comput. Chem.* **2011**, *32*, 1456−1465.
(26) Andersen, M.; Medford, A. J.; Nørskov, J. K.; Reuter, K. Scaling-Relation-Based Analysis of Bifunctional Catalysis: The Case for Homogeneous Bimetallic Alloys. *ACS Catal.* **2017**, *7*, 3960−3967.
(27) Molero, H.; Stacchiola, D.; Tysoe, W. T. The Kinetics of Ethylene Hydrogenation Catalyzed by Metallic Palladium. *Catal. Lett.* **2005**, *101*, 145−149.
(28) Chou, P.; Vannice, M. A. Benzene Hydrogenation over Supported and Unsupported Palladium 0.2. Reaction Model. *J. Catal.* **1987**, *107*, 140−153.
(29) Aboul-Gheit, A. K.; Abdel-Hamid, S. M.; Aboul-Fotouh, S. M.; Aboul-Gheita, N. A. K. Cyclohexene Hydroconversion Using Monometallic and Bimetallic Catalysts Supported on Gamma-Alumina. *J. Chin. Chem. Soc.* **2006**, *53*, 793−802.
(30) Aramendia, M. A.; Borau, V.; Jimenez, C.; Marinas, J. M.; Moreno, A.; Urbano, F. J. Dehydrogenation of Cyclohexane over Supported Pd Catalysts 0.2. Influence of the Support and Reduction Temperature. *React. Kinet. Catal. Lett.* **1995**, *56*, 87−96.
(31) Morin, C.; Simon, D.; Sautet, P. Intermediates in the Hydrogenation of Benzene to Cyclohexene on Pt(111) and Pd(111): A Comparison from Dft Calculations. *Surf. Sci.* **2006**, *600*, 1339−1350.
(32) Lehwald, S.; Ibach, H.; Demuth, J. E. Vibration Spectroscopy of Benzene Adsorbed on Pt(111) and Ni(111). *Surf. Sci.* **1978**, *78*, 577−590.
(33) Saeys, M.; Reyniers, M. F.; Marin, G. B.; Neurock, M. Density Functional Study of Benzene Adsorption on Pt(111). *J. Phys. Chem. B* **2002**, *106*, 7489−7498.
(34) Tysoe, W. T.; Nyberg, G. L.; Lambert, R. M. Structural, Kinetic, and Reactive Properties of the Palladium(111)-Ethylene System. *J. Phys. Chem.* **1984**, *88*, 1960−1963.
(35) Steininger, H.; Ibach, H.; Lehwald, S. Surface-Reactions of Ethylene and Oxygen on Pt(111). *Surf. Sci.* **1982**, *117*, 685−698.
(36) Sabbe, M. K.; Lain, L.; Reyniers, M. F.; Marin, G. B. Benzene Adsorption on Binary Pt3m Alloys and Surface Alloys: A Dft Study. *Phys. Chem. Chem. Phys.* **2013**, *15*, 12197−12214.
(37) Heard, C. J.; Hu, C. Q.; Skoglundh, M.; Creaser, D.; Gronbeck, H. Kinetic Regimes in Ethylene Hydrogenation over Transition-Metal Surfaces. *ACS Catal.* **2016**, *6*, 3277−3286.
(38) Montemore, M. M.; Medlin, J. W. A Unified Picture of Adsorption on Transition Metals through Different Atoms. *J. Am. Chem. Soc.* **2014**, *136*, 9272−9275.
(39) Bratlie, K. M.; Lee, H.; Komvopoulos, K.; Yang, P. D.; Somorjai, G. A. Platinum Nanoparticle Shape Effects on Benzene Hydrogenation Selectivity. *Nano Lett.* **2007**, *7*, 3097−3101.

DOI: 10.1021/acs.jpcc.8b09564
J. Phys. Chem. C 2019, 123, 8370−8378